LANGMUIR

Invited Feature Article

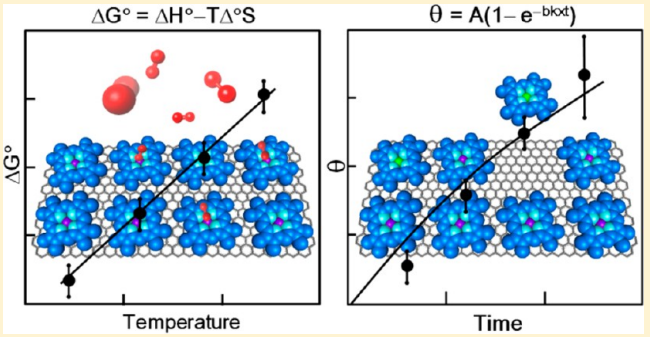
pubs.acs.org/Langmuir

Kinetic and Thermodynamic Control in Porphyrin and Phthalocyanine Self-Assembled Monolayers

K. W. Hipps* and Ursula Mazur

Department of Chemistry and Materials Science & Engineering Program, Washington State University, Pullman, Washington 99163-4630, United States

ABSTRACT: Porphyrins and phthalocyanines are ubiquitous in modern science and technology. Their stability, redox properties, and photoresponse make them candidates for numerous applications. Many of these applications rely on thin films, and these are critically dependent on the first monolayer. In this article, we focus on noncovalently bound self-assembled monolayers of porphyrins and phthalocyanines at the solution−solid interface with special emphasis on the kinetic and thermodynamic processes that define the films and their reaction chemistry. We first discuss the difference between film-formation kinetics and desorption kinetics from fully formed films. We then present evidence that many of these monolayers are controlled by adsorption kinetics and are not in thermodynamic equilibrium. Measurement of the solution−solid interface desorption energy by scanning tunneling microscopy is discussed, and data is presented for cobalt, nickel, and free base octaethylporphyrin. The activation energy for the desorption of these compounds into phenyloctane is about half of the computed desorption energy in vacuum, and this is discussed in terms of the role of the solvent. Preexponential factors are very low compared to desorption into vacuum, and this is attributed to a reduction in the entropy of activation due to the participation of solvent in the transition state. An example of the use of relative desorption kinetics to create a new binary surface structure is given. It is suggested that this is a synthesis route that may have been missed because of the large difference in solution concentrations required to drive binary film formation. Attention then turns to the axial reaction chemistry of metalloporphyrins and metallophthalocyanines supported on conducting surfaces. We show several examples of chemistry unique to the supported complexes: cases where the metal binds ligands more readily and cases where the substrate induces ligand loss. Understanding this new axial coordination chemistry is of great importance in catalysis, sensing, and the growth of 3D materials from a self-assembled template.



Downloaded via LBRY FOR NATURAL SCIENCES RAS on September 3, 2018 at 10:51:43 (UTC).
See https://pubs.acs.org/sharingguidelines for options on how to legitimately share published articles.

1. INTRODUCTION

Why Study Phthalocyanines and Porphyrins? Phthalocyanines (Pc) (Figure 1 left) and porphyrins (P) (Figure 1 right) are macrocyclic compounds formed with 16-membered rings. The rings are formed from the covalent linking of four pyrrole-like compounds (pyrrole for porphyrins and isoindole for phthalocyanine). These highly conjugated systems produce deeply colored compounds with optical band gaps usually falling in the 1 to 2 eV range and with oxidation and reduction potentials within about 1 eV of the saturated calomel electrode (SCE). Even more exciting, the optical electronic, chemical, and mechanical properties of these compounds can all be tuned by chemical substitutions at the peripheral (p) and nonperipheral (np) positions in phthalocyanine and the β and meso positions in porphyrins or by changing the central metal for either system. Although the central metal is often associated with divalent ions, stable complexes of higher-valence ions with axial substituents (such as halides of Fe^{3+} or vanadyl) are well known. The so-called free bases have two protons replacing the metal ion, and even dilithium complexes are known.[1,2]

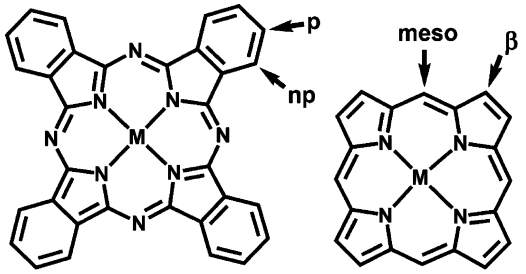


Figure 1. Molecular structures of a phthalocyanine (left) and a porphyrin (right). Substitutions can be placed at any of the positions indicated or axially through coordination to the central metal.

As one might expect, the ability to create a wide range of substituted complexes also results in a wide range of solubility. Thus, porphyrin and phthalocyanine complexes can be deposited on surfaces by adsorption or spin-casting from solution. Many of the smaller derivatives (and the parent compounds) are stable

Received: July 31, 2017
Revised: September 1, 2017
Published: September 20, 2017

 © 2017 American Chemical Society

DOI: 10.1021/acs.langmuir.7b02672
Langmuir 2018, 34, 3−17

above their sublimation point and can be vapor deposited in a manner similar to that of many inorganic compounds. Most are reasonably stable with respect to atmospheric or radiation exposure, and the phthalocyanines are especially so. These materials have such a wide range of interest that there is a journal[1] dedicated to them and an extensive series of volumes chronicling their properties.[2]

Because of the properties outlined above, these materials are either currently found in or proposed for use in a wide range of modern devices and technologies.[3] These include but are not limited to solar cells,[4−6] chemical sensors,[7−9] medicine,[10−12] optoelectronics,[13−16] catalysts,[17−19] and FETs.[20−22] For many of these applications, the preferred form of the compound is as a film. The electronic and mechanical properties of these films can, to a great extent, depend upon the structure of the first layer that forms the foundation for the interface between the support and the film.[23−31] Thus, in order to get optimal control over the properties of the desired device, the ability to rationally design the first monolayer of material is essential. One route to designer monolayers is through self-assembly.[32−42]

Self-Assembly. Although there are many examples of P and Pc systems covalently bound to substrates,[43−45] this review will focus on those that are not covalently bound. Rather, we focus on systems where the surface−adsorbate interaction is weak enough that the adsorbate−adsorbate interactions are competitive. In vacuum-deposited films, self-assembly is the formation of well-ordered films of a particular molecular structure that result from a balancing of adsorbate−adsorbate forces and adsorbate surface interactions. An early example of this in the case of porphyrins and phthalocyanines was given by Hipps.[33] In that case, fluorine−hydrogen bonding was used to create a binary structure where each cobalt Pc was surrounded by four nickel tetraphenylporphyrins (TPP). In the case of the solution−solid interface, self-assembled surface structures are formed through a delicate balance between the intermolecular interactions of the components forming the adlayer (tectons), the tecton−surface interactions, the solvent−tecton interactions, and the solvent−surface interactions. If the intermolecular interactions are too strong, then island growth of molecular multilayers, growth of a pure tecton having a typical crystal plane as the surface, and/or phase segregation (in the case of more than one tecton) can occur. If the tecton−surface interactions are too strong, then the film structure is completely defined by the surface reactive sites and the ability to tune the surface structure is lost. If the solvent-tecton interactions are too strong, a well-defined adlayer does not form, or perhaps an adlayer forms that incorporates the solvent. Similarly, if the solvent surface interactions are strong compared to the tecton−surface interactions, no tecton adlayer (or an incomplete tecton adlayer) forms. In some systems, there can be more than one surface structure (polymorph) that can form. The surface structure in these cases can sometimes be controlled by varying the concentration, temperature, or solvent.[71] In this article, we will focus on the adsorption of P and Pc molecules at the solution−solid interface.

Consider, for example, the case of adsorption of vanadyl (VO^{+2}) and free base 2,9,16,23-tetraphenoxy-29*H*,31*H*-phthalocyanine (PcPhO) on highly oriented pyrolytic graphite (HOPG) from 1-phenyloctane (PO).[46] Scanning tunneling microscopy (STM) images taken from these systems are shown in Figure 2. The free base forms an oblique monolayer that is incommensurate with the underlying graphite lattice, and VOPcPhO can form three different polymorphs depending on solution concentration, all of which are commensurate with the graphite lattice.

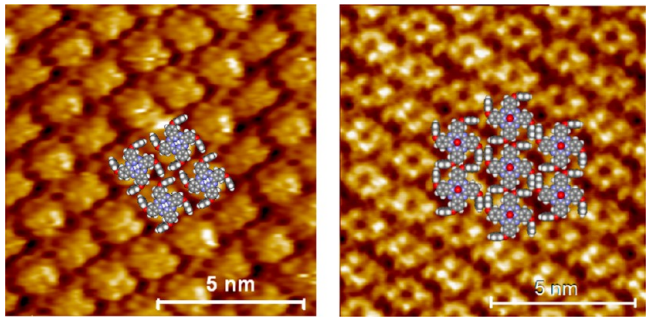


Figure 2. STM comparison of monolayers formed at the HOPG/1-phentloctane interface. On the left is H_2PcPhO (rectangular lattice), and on the right is VOPcPhO (hexagonal lattice).

The VOPcPhO structure shown in Figure 2 is a hexagonal structure. Mazur et al. attribute this difference to the dipole moment normal to the surface in the vanadyl complex preferentially interacting with a particular site on the highly oriented pyrolytic graphite (HOPG) surface. Although no solvent dependence was reported for the PcPhO system, there is a rich body of literature of scanning tunneling microscopy (STM) studies showing that the choice of solvent does produce structural variations in the self-assembled film.[47−52] For later use, note that the STM image of the vanadyl group appears as a dark center in the complex.

Porphyrins and phthalocyanines can be used to form self-assembled monolayers both as their parent complexes and as derivatives. Some of the first single-molecule systems to be observed by ultrahigh vacuum (UHV) STM were metal phthalocyanines (MPc) and metal porphyrins (MP), and they remain of strong interest.[53−56] A popular way to create patterned porphyrin and phthalocyanine monolayers at the solution−solid interface, for example, has been to attach long alkane chains and use the chain interdigitation to define the MPc or MP spacing.[57,58] Many other substituents have been used to create patterned MP and MPc layers.[46,48,59] On most metal surfaces, P and Pc will form islands at submonolayer coverage. On HOPG, however, it is essential either to have the P ring immediately on the surface or for there to be peripheral groups that provide anchoring; otherwise, the porphyrins tend to be very mobile on the HOPG surface at room temperature. Tetraphenylporphyrin (TPP) is an example of a porphyrin that is mobile on the HOPG surface.

Why STM? Unlike adlayers formed that are stable in vacuum where transmission electron microscopy (TEM), selected-area electron diffraction (SAED), low-energy electron diffraction (LEED), X-ray diffraction, and STM can be used to probe the film structure, only STM can be used to provide the molecular structure of thin films and monolayers at the solution−solid interface. Fortunately, it turns out to be an exceptionally good tool for submolecular resolution[35,39,40,46−51] and a useful tool for chemical specificity.[60−65] Although the resolution achieved in solution is seldom as good as that seen in UHV, it is usually sufficient to distinguish similarly sized molecules having different shapes. This ability to distinguish some of the internal structure of adsorbed molecules is often referred to as submolecular resolution. Also of great value is the variation in contrast seen with different moieties (e.g., −OH, −Cl, −Br, and −I)[62] and with different metal ions (e.g., Fe^{2+}, Co^{2+}, Ni^{2+}, and VO^{+2}).[46,55,60,61] These two attributes of solution-phase STM—submolecular resolution and chemical specificity—allow for a detailed determination of the surface structures of adlayers formed

DOI: 10.1021/acs.langmuir.7b02672
Langmuir 2018, 34, 3−17

from one or multiple components. For example, Figure 3 shows the STM image of a well-ordered 1:1 composition self-assembled

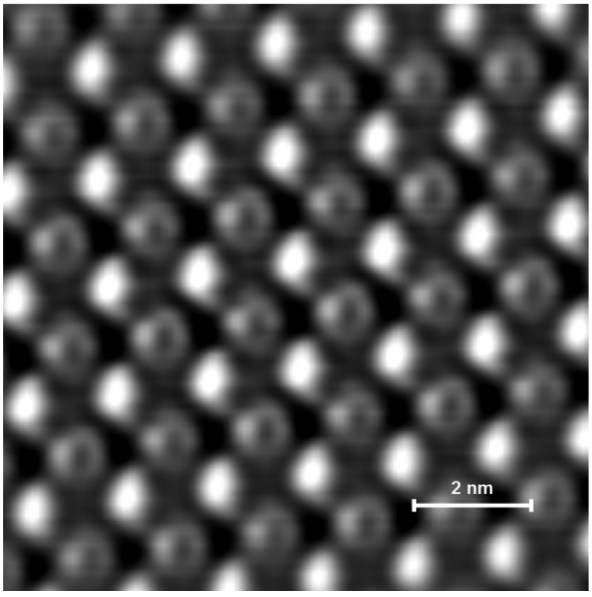


Figure 3. STM image of a CoTPP-coronene self-assembled monolayer on Au(111). The CoTPP's are the bright molecules. The rectangular unit cell has parameters of A = 1.73 nm and B = 1.56 nm.[66]

monolayer (SAM) formed from CoTPP and coronene obtained at the PO/Au(111) interface.[66] The CoTPP molecule has a bright appearance because of the cobalt ion at its center, whereas the coronene appears as a ring. Although spatially averaged techniques such as Raman and UV−vis could determine the composition at the interface, they could not differentiate among phase segregation, a random distribution, or a structured adlayer. They certainly could not provide the detailed structure seen in Figure 3.

Although much of the solution−solid STM work to date has been performed in nonconducting solutions such as PO, alkane acids, and alkanes, it is by no means required. In fact, there is a healthy body of literature on STM studies in the electrochemical environment.[67−69] Thus, virtually any solution−solid interface is accessible by STM methods.

Adsorption and Desorption at the Solution−Solid Interface. It is useful to contrast the major differences between well-studied adsorption by vacuum deposition and deposition from solution. The solvent plays a key role in all phases of the adsorption and desorption processes at the solution−solid interface, but most obvious is the fact that it is possible for adsorbed molecules making up the self-assembled structure (tectons) to dynamically exchange between surface and solution whereas those adsorbed in vacuum either stick or they do not. Obvious consequences of this exchange are the possibility to heal defects in the adlayer and to anneal the film to create higher-density structures.

In reality, the solvent plays a role in every step of the thermodynamics and kinetics of adlayer formation at the solution−solid interface.[70−72] Consider the Born−Haber cycle (Figure 4) proposed by Lackinger and co-workers to describe the enthalpy of adsorption from solution in terms of the enthalpy of adsorption from vacuum.[70] Lackinger defined ΔH_{dewet} as the enthalpy cost of solvent desorption from the adsorbate monolayer. A set of relationships paralleling Figure 4 can be

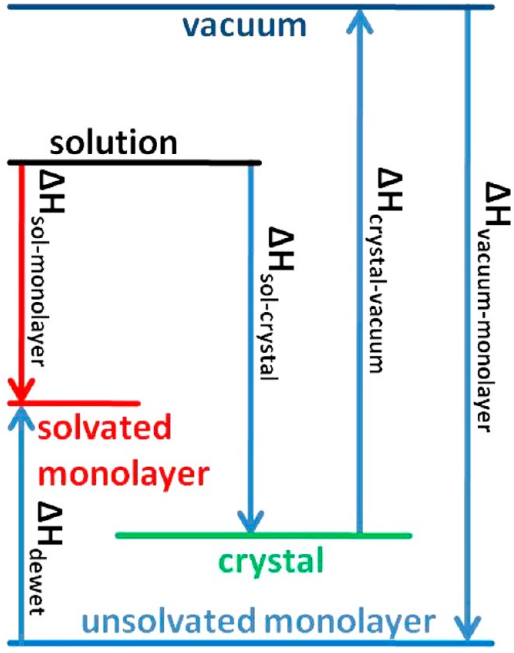


Figure 4. Scheme for the Born−Haber cycle of adsorption as proposed by Lackinger. Reprinted with permission from ref 70. Copyright 2013 American Chemical Society.

written for the entropy and Gibbs free energy of adsorption. Note that the change in state function during the dissolution of the pure crystalline tecton and the change in state function for wetting the monolayer can depend strongly on the solvent, and thus ΔH, ΔS, and ΔG of adsorption from solution can vary significantly from the values observed and calculated for vacuum adsorption. It is worth noting that the value of ΔS for adsorption from vacuum is always negative, whereas that from solution may have either sign depending upon the number and organization of solvent molecules that must be displaced to form the monolayer. Note also that Figure 4 relates to the adsorption of a single species forming a single polymorph. It can, of course, be generalized to multiple components and polymorphs.

Just as the presence of solvent complicates the adsorption thermodynamics, it also significantly affects the kinetics of the SAM growth process. Figure 5 presents a schematic (and simplified) representation of the potential energy surface experienced by a tecton during the SAM formation (and dissolution) process. Like Figure 4, Figure 5 considers only a single adsorbate forming a single polymorph. Also, like Figure 4, it can be generalized. From the left, one can follow a tecton adsorbing onto a substrate with nearly zero surface coverage of SAM. Unlike vacuum deposition where the activation energy of adsorption, E_{a1}, is often negligible, there can be a significant barrier associated with solvent stripping from a portion of the tecton and from the substrate surface.[72,73] Once the tecton is on the (low-coverage) surface, it has a periodic barrier to diffusion associated with the surface lattice structure and a stochastic barrier caused by the need to displace solvent from the surface onto which it is moving.[74] E_{d1} is the average activation barrier these diffusing tectons must surmount to return to solution. Unlike the vacuum adsorption case, it is possible for stable adsorption to occur even if E_{d1} is less than E_{a1} provided that a single tecton is displacing a number of well-ordered solvent molecules from the surface (e.g., $\Delta S_{ads} \gg 0$). As the surface concentration increases, islands of SAM will form. As a tecton on

DOI: 10.1021/acs.langmuir.7b02672
Langmuir 2018, 34, 3−17

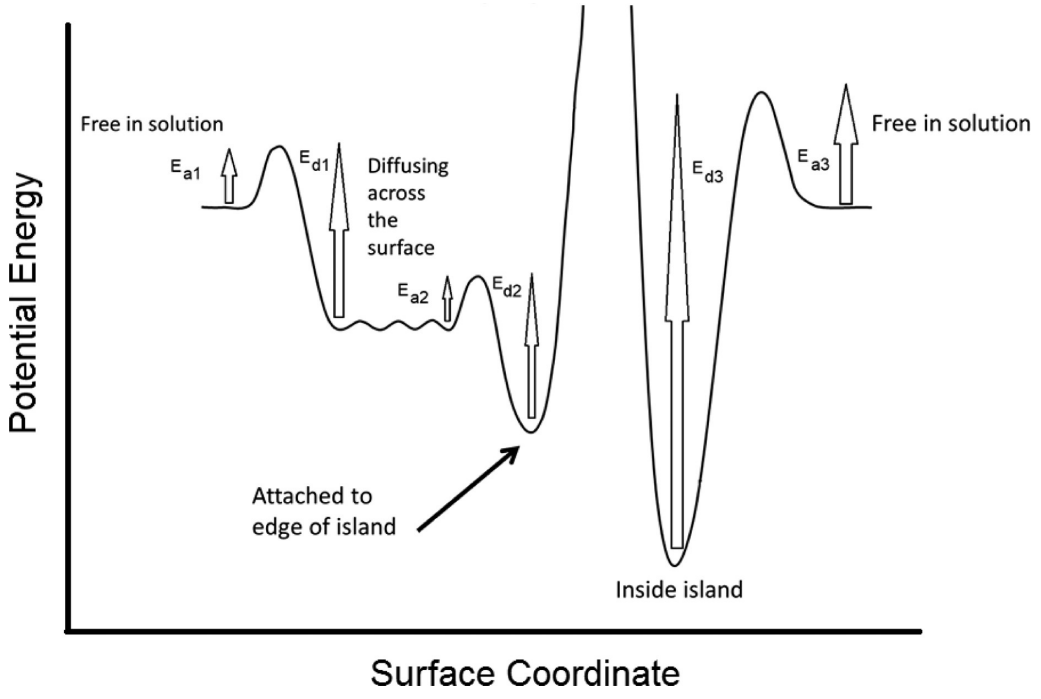


Figure 5. Cartoon of potential energy surface seen by a single tecton surrounded by solvent as it moves from the solution to a solid surface. Only one polymorph is considered. The tecton proceeds to the right where it surmounts a small activation barrier in order to attach to the edge of a self-assembled growing island. Once the tecton has been incorporated into a well-structured SAM, it can move back into solution by surmounting activation barrier E_{d3}.

the low-coverage surface approaches such an island, it will again face an activation barrier for attachment to the island boundary, E_{a2}. The height of this barrier will contain a significant component from solvent reorganization. Separation from the island edge and return to diffusion across the surface require activation energy E_{d2}. As long as E_{d2} is significantly less than E_{d1} and the activation entropies are not too different, desorption from the low-coverage surface will be the rate-limiting step.

The very sharp increase in potential energy near the center of Figure 5 is for a molecule attempting to burrow into the interior of an existing island. A tecton can, however, directly desorb from the interior of a SAM, or it can adsorb from solution into a single tecton vacancy. These actions are associated with activation energies E_{d3} and E_{a3}. For most SAMs, there is an increase in energetic stability for the tecton incorporated into the body of the SAM relative to an island edge or isolated on the surface. Thus, E_{d3} is shown to be larger than E_{d2} or E_{d1}.

Assuming that each of these desorption steps is first order in the appropriate species per unit area (number of diffusing tectons, number of perimeter tectons, and number of tectons within islands), one can define a rate constant for each process, k_{di}, $i = 1-3$. Eyring's absolute rate theory[75] gives eq 1, where $\Delta S^{\dagger}$ is the entropy of activation and $\Delta H^{\dagger}$ is the activation enthalpy, which for condensed phases is nearly the activation energy. With assumptions of a not too wide temperature range and condensed phases, one has the familiar Arrhenius equation, eq 2.

$$k_{di} = \frac{kT}{h} e^{\Delta S^{\ddagger}/R} e^{-\Delta H^{\ddagger}/RT} \approx k_{di} = \frac{kT}{h} e^{\Delta S^{\ddagger}/R} e^{-E_{di}/RT} \quad (1)$$

$$k_{di} \approx k_{di}^{0} e^{-E_{di}/RT} \quad (2)$$

Although the model depicted in Figure 5 is perhaps the simplest possible case, even this simple model gives at least two adsorption and desorption mechanisms. These processes will have generally different rate constants. Moreover, the number of tectons that can utilize a particular mechanism will depend upon the coverage. Thus, we should expect desorption rate expressions to depend on coverage in more than the trivial form of rate = $-k_d\theta$, where θ is the fraction of surface covered. Certainly, the desorption rate from a nearly full monolayer will be different from that of a sparsely covered surface. Often, the adsorption rate is given by $k_{ai}c$, where c is the molar concentration of tecton in solution. The difference in adsorption rates with coverage will depend upon the difference in activation energies E_{a1} and E_{a3} and the associated $\Delta S_i^{\dagger}$.

Extracting correct mechanisms for such complicated processes from ensemble measurements (e.g., amount adsorbed or optical absorbance) is extremely difficult. Ensemble methods can provide data on the concentration and temperature evolution of the system on a relatively fast time scale, but methods that allow direct tecton scale monitoring (such as STM) can provide definitive mechanistic insights. Single-molecule measurements, however, must be made a large number of times in order provide rates and equilibrium constants relevant to ensemble averages.

2. KINETIC VERSUS THERMODYNAMIC CONTROL IN PORPHYRIN AND PHTHALOCYANINE MONOLAYER FORMATION

For SAMs at the solution−solid interface, deciding if the observed structure is in fact in thermodynamic equilibrium with the solution is a nontrivial issue.[71] Often in the literature, systems are assumed to be in equilibrium without verification. Sometimes simple but inconclusive tests (such as invariance of the structure to minor heating) are applied. Unfortunately, evidence is mounting that kinetics often dominates in determining the SAMs formed on surfaces near room temperature.[71] To determine if a particular system is at thermodynamic equilibrium, one must discover the answers to three questions:

(1) Are tectons exchanging between surface and solution?

DOI: 10.1021/acs.langmuir.7b02672
Langmuir 2018, 34, 3−17

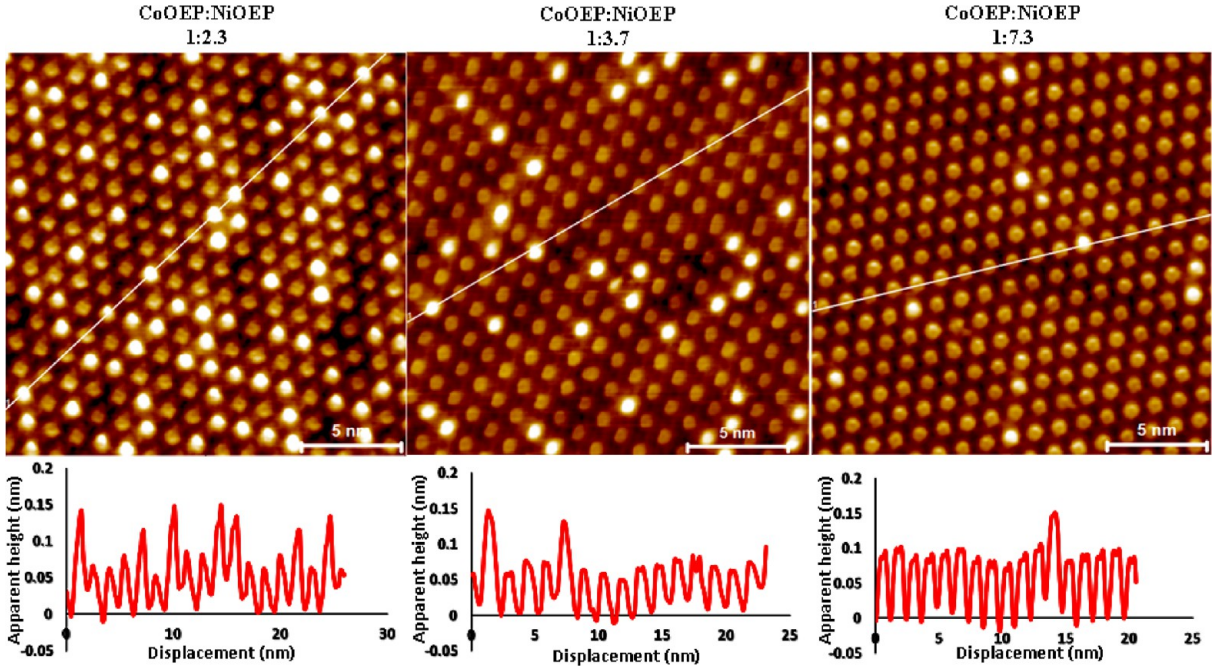


Figure 6. STM images resulting from adsorption from various ratios of CoOEP to NiOEP in PO solution onto Au(111) at 20 °C. STM images were obtained under set-point conditions of −0.7 V sample bias and 20 pA. Reprinted with permission from ref 78. Copyright 2014 American Chemical Society.

(2) Is the system at steady state?

(3) Is the state of the system independent of history? That is, does a change in system concentration or temperature result in the same state as when the sample is initially prepared with those parameters?

A "no" answer to any of these questions guarantees that the as-prepared system is not in thermal equilibrium and that a thermodynamic analysis is not appropriate. There is also the case where ΔG° is so large and negative that the rate of desorption becomes very much less than the rate of adsorption. If the surface is near monolayer coverage, on a time scale long with respect to the adsorption time it will become impossible to distinguish the exchange between solution and surface. Further, small changes in solution concentration may not suffice to shift the observed surface concentration. In general, we advise caution in assigning kinetic or thermodynamic control when dealing with adsorption events with large computed equilibrium constants. In Langmuir adsorption, for example, if a monolayer forms in 1 s at a solution concentration of 10^{-5} M, desorption rates at room temperature would be of the order of 1/hr for ΔG° of the order of −50 kJ/mole.

Of course, the issue of applicability of equilibrium thermodynamics is always a question of time scale. Hydrogen and oxygen after the introduction of a catalyst come to equilibrium (water) rather quickly, but on a time scale of nanoseconds, it is a kinetic system. In this work, we are referring to the time scale of the experiments (seconds to months).

An example of the qualitative assessment of the role of kinetics in porphyrin self-assembly comes from the work of Coenen and co-workers,[76] who reported on copper 5,10,15,20-tetraundecylporphyrin ((TUP)Cu), at the octanoic acid−HOPG interface. These substituted porphyrins quickly form large domains of well-ordered molecules with heavily interdigitated alkyl chains. They assemble into not one but two surface polymorphs. The prevalence of each polymorph depends on solution concentration, with the denser polymorph being more common in higher-concentration solutions. One might attribute this to a simple concentration-dependent equilibrium between two polymorphs. Such is not the case. If one prepares the low-density phase and then covers it with high-concentration solution, then regions of the low-density phase persist even after 16 h. This demonstrates that the surface molecular structures are not in equilibrium with the solution but rather are determined by the kinetics of the original adsorption process.

By exposing the (TUP)Cu low-density surface to a solution of (TUP)Co, the authors were able to both prove their assertion of kinetic control and identify the mechanism of the very slow equilibration process.[76] Cobalt porphyrins and phthalocyanines are well known to appear to have very bright centers in STM images at moderate voltages, whereas copper and nickel porphyrins and phthalocyanines appear dark.[55,60,77] If there is exchange between the surface and solution, then the bright cobalt porphyrins should replace the dim copper complexes at the rate of the exchange. What is observed is a very slow buildup of (TUP)Co only in the vicinity of certain defects in the low-density phase. Insertion into regions that are defect-free occurs in only 2 to 3% of the total cobalt insertion sites. Thus, the primary mechanism for adlayer formation is the initial adsorption and nucleation of the TUP species from solution. Once the initial monolayer forms, the desorption rate from within an island (dependent on E_{d3}) is very slow. Exchange with solution can occur only at finite rates in regions where E_{d1} controls the desorption process, that is, at grain boundaries and surface defects.

As interesting as this revelation is, it leaves several questions unanswered. Does the slow desorption rate depend upon the alkyl chains of the TUP? What are the rates of desorption themselves? In particular, what are the rates and activation energies associated with each of the processes shown in Figure 5?

Consider the binary porphyrin system composed of cobalt octaethylporphyrin (CoOEP) and NiOEP on Au(111).[78] These

DOI: 10.1021/acs.langmuir.7b02672
Langmuir 2018, 34, 3−17

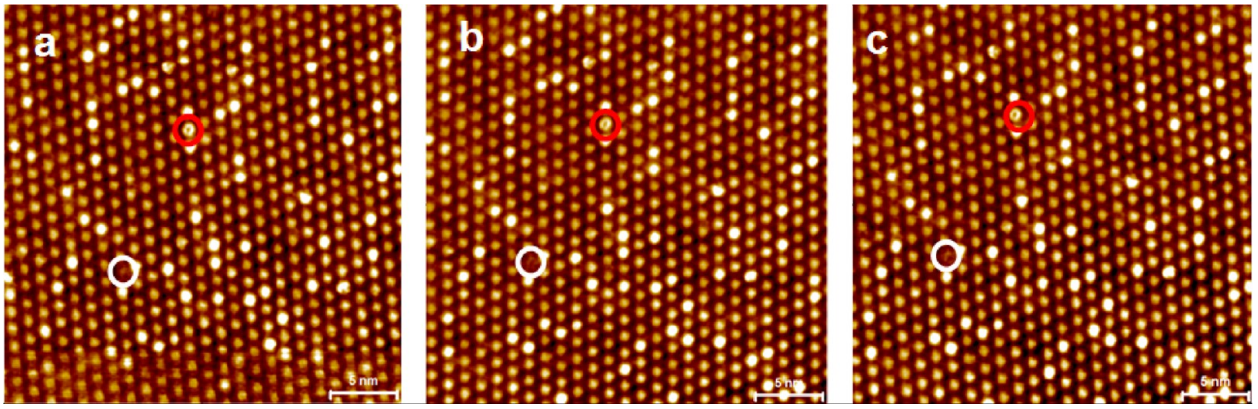


Figure 7. Sequential STM images taken from a monolayer formed on HOPG from contact with a solution having $X_N = 0.79$. Images are taken about 2.5 min apart in time. The set point was −0.7 V and 20 pA. Reprinted with permission from ref 78. Copyright 2014 American Chemical Society.

systems have very short alkane chains that are known to turn up away from the surface,[79] minimizing the role of substituents in the adsorption energy. Figure 6 presents STM images obtained when solutions of CoOEP and NiOEP in PO (in different concentration ratios) are allowed to come to steady state with a Au(111) surface. At the concentrations used, a dense monolayer quickly forms. One can easily distinguish the CoOEP (bright) from the NiOEP (dim). By directly counting the number of bright and dark molecules within a given area, one can arrive at the relative surface coverage of NiOEP on the surface, θ_N. A plot of θ_N versus the mole faction of NiOEP (X_N) relative to the total number of moles of metal octaethylporphyrin (MOEP) at five different values of X_N gave a straight line with a slope of 1 ($\theta_N = X_N$). On the basis of this evidence alone, one would be tempted to assume that the system was in equilibrium and that the free energies of adsorption were the same for NiOEP and for CoOEP. This is not, however, the case.

If one monitors a given region of the surface as a function of time, then one finds that, at temperatures below 70 °C, no CoOEP exchanges for a NiOEP and vice versa. This can be seen, for example, in a series of images shown in Figure 7 that were taken at 25 °C and about 150 s apart. There are two defects in the monolayer (circled in red and white) that allow one to track individual molecules despite the thermal drift in the images. If exchange with solution were occurring, then blinking would be observed in the sequence of images as CoOEP exchanges for NiOEP. Only at temperatures above 100 °C does measurable exchange begin to occur. Thus, the equality between θ_N and X_N is due to equal adsorption rate constants (associated with E_{a1}) and an orders of magnitude slower desorption rate, not to equal free energies of adsorption.[78] This later statement is further justified by the fact that the complete monolayer forms in less than 10 s of exposure of the gold to a solution of either CoOEP or NiOEP.[78]

To make quantitative measurements on the desorption rate of CoOEP from the Au(111) surface and to extract the desorption rate constant associated with E_{d3} in Figure 5, NiOEP was used as a tracer. A solution of X_N of a fixed large value was placed into contact with an initially full monolayer of pure CoOEP at 135 °C, and θ_N was measured as a function of time. The experiments were conducted in a series of steps where the solution was heated for a fixed time, cooled quickly to room temperature for measurement of θ_N, and then reheated for the next period. (If there is an error introduced by this process, it would make the reported desorption rates too fast.) The resulting plot of θ_N versus time was exponential and did not reach half of the saturation (equilibrium) concentration of NiOEP even after 3 h of heating at 135 °C. A simple model was proposed to account for the exponential form of the curve.[71,78] Adsorption rates were taken to be orders of magnitude faster than desorption rates. The rate of appearance of NiOEP on a full monolayer containing both Ni and Co sites was set equal to (the rate of disappearance of Co times the probability that the site will be filled by Ni) − (the rate of disappearance of Ni times the probability that it will be replaced by Co). On the basis of the fact that $X_N = \theta_N$ for initial monolayer formation, the rate of site filling by species i was taken to be proportional to X_i.

The resulting expression for the fractional surface coverage at time t is

$$\theta_N = \left(\frac{1}{b}\right)(1 - e^{-bk_C X_N t}) \tag{3}$$

where

$$b = \left[\left(\frac{k_N^d}{k_C^d X_N}\right)(1 - X_N)\right] + 1 \tag{4}$$

The rate constant for desorption of NiOEP from the complete monolayer is k_N^d, and k_C^d is the corresponding value for CoOEP. In this article, the authors were unable to distinguish a difference between k_C^d and k_N^d. They found $k_C^d = 6.7 \times 10^{-5}$ s^{-1} at 135 °C. This rate constant is surprisingly small. Consider for example the desorption rate constant for 1-octadecanethiol from Au in hexane. Karpovich and Blanchard[80] have reported a value of 0.2 s^{-1} at 20 °C, and Campbell[81] says that a value of 10^{-4} s^{-1} is more appropriate. Long-chain thiols are well known for forming stable SAMs based on both covalent bonding between sulfur and gold and van der Waals interactions between alkane chains. The fact that the desorption rate constant for the noncovalent adsorption of CoOEP at 135 °C is at least 1 order of magnitude smaller than that of 1-octadecanethiol at 20 °C indicates that the MOEP−Au interaction is much stronger than expected.

Having proven that desorption rate constants could be extracted from time- and temperature-dependent STM images, Hipps and co-workers turned their attention to extracting the actual activation energies and preexponentials for desorption. In a series of studies using PO as the solvent and HOPG as the substrate, they measured the temperature-dependent desorption rates from mixed monolayers of CoOEP, NiOEP, and H_2OEP.[82,83] They used eqs 3 and 4 to fit data taken at several different temperatures. Initially, monolayers were either pure

DOI: 10.1021/acs.langmuir.7b02672
Langmuir 2018, 34, 3−17

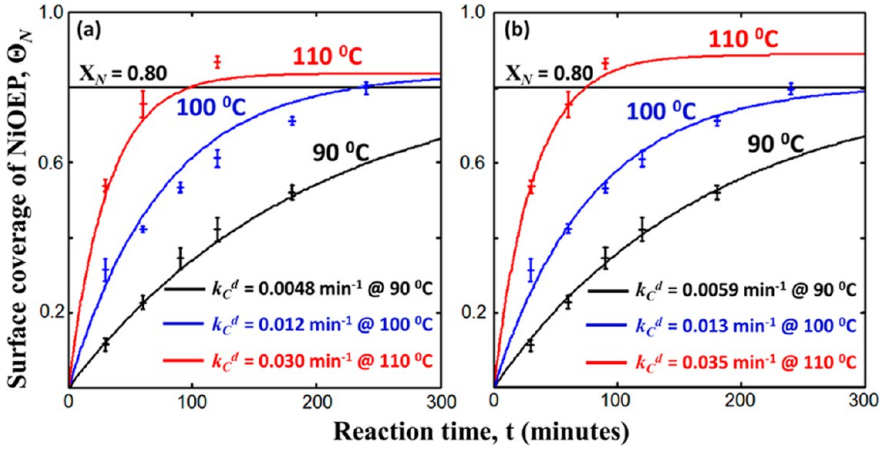


Figure 8. (a) Best-fit curves for surface coverage of NiOEP, $\theta_N$on HOPG, with reaction time and average k_C^d values at 90 °C (black curve), 100 °C (blue curve), and 110 °C (red curve), and optimized values of ΔE_C, ΔE_N, and k_C^0 for the entire time (t/min) and temperature (T/°C) data set. (b) Optimized values of k_C^0 and K^d at each T. Reproduced from ref 82. Copyright 2015 American Chemical Society.

CoOEP or pure H_2OEP, which were then exposed to high-concentration solutions of another OEP species as a function of temperature and time. Representative data for the case of CoOEP exposed to X_N = 0.80 is presented in Figure 8 and is taken from ref 82. In this case, data were fit in two different ways: (a) eq 2 was used in place of the individual rate constants in eq 3 and all the data were used to fit the energies and preexponentials and (b) each isotherm was fit to eq 3 and the individual observed rate constants were plotted versus $1/T$ to extract activation energies and preexponentials. The two approaches gave similar results. Note that the predicted equilibrium surface coverage of NiOEP is slightly greater than for CoOEP, indicating that $\Delta G°$ for the adsorption of NiOEP from HOPG is slightly more negative than for CoOEP.

Values obtained for k_{d3}^0 and E_{d3} are collected in Table 1. Error bars for the preexponentials are large, but this is not unusual for

Table 1. Preexponential Factors and Activation Energies for the Desorption of Octaethylporphyrins in 1-Phenyloctane from HOPG Using OEP Tracers (in Parentheses)[a]

	CoOEP (NiOEP)	CoOEP (H_2OEP)	H_2OEP (CoOEP)
k_{d3}^0 (s^{-1})	$(4 \pm 3) \times 10^{14}$	$(2 \pm 1) \times 10^{14}$	$(3 \pm 2) \times 10^{14}$
E_{d3} (kJ/mol)	105 ± 5	126 ± 4	125 ± 4

[a]Data are taken from refs 82 and 83.

desorption data where even in UHV desorption uncertainties are often specified to the power of tens.[84] The values of k_{d3}^0 are surprisingly small in comparison to those expected for desorption into vacuum. If one uses eq 1, then these values correspond to a $\Delta S^{\ddagger}$ of only about 35 J/mol·K. One can estimate the CoOEP-only (no solvent involvement) contribution to the desorption entropy in solution to be about 350 J/mol·K,[85] and the $\Delta S^{\ddagger}$ (CoOEP only) to be about 270 J/mol·K.[75,84] Although these estimated values are rough, they are still an order of magnitude larger than required to account for the observed preexponential factor. These estimates were based on the assumption that the solvent neither adsorbs on HOPG nor solvates CoOEP. We believe that these assumptions are not appropriate, and we attribute the small value of entropy of activation to the critical role the solvent plays in the activated complex.

The desorption activation energies from HOPG for CoOEP, NiOEP, and H_2OEP in PO are within 10% of each other and correspond to about 125 kJ/mol. The actual desorption energy will be less than this by E_{a3}, but we ignore that difference for now. Because the solution-phase adsorption involves a tiny change in volume at 1 atm, the energy of adsorption and the enthalpy of adsorption are essentially the same. DFT calculations for the energy required for the desorption of CoOEP from HOPG into vacuum predict 230 kJ/mol resulting in an enthalpy of adsorption of −232 kJ/mol.[86] With reference to Figure 4, values of the heat of solution, the heat of sublimation, and the heat of dewetting are required to reconcile these two desorption energies. The heats of sublimation and solution are fairly easy to measure.[70] The heat of solution for CoOEP in PO is about 18 kJ/mol,[87] and the heat of sublimation is about 100 kJ/mol.[88] The value that is extremely hard to determine for cases where the solvent does not strongly order on the surface is the heat of dewetting. The heat of dewetting turns out to be one of the least-known values in self-assembly, and both theoretical and experimental efforts are underway to determine representative values. In any case, for the PO/OEP/HOPG system, it is unlikely that the dewetting enthalpy will be less than −20 kJ/mol or more than 20 kJ/mol.[89] Using all of the above values and Figure 4, the enthalpy of adsorption in vacuum should be (−125 − 100 + 18 ± 20) kJ/mol or −207 ± 20 kJ/mol, in good agreement with the value computed by DFT. In this calculation, we have misused the activation energy E_{d3}. The energy of desorption is more properly $E_{d3} - E_{a3}$ and corrected for the difference in thermal energy stored in the products and reactants at 293 K. Thus, we have overestimated ΔH_{ads}^{sol}.

Only the overall rate constant was reported for the desorption of CoOEP from Au(111). If one makes the assumption that the preexponential factor for gold is similar to HOPG, then one finds that E_{d3} for CoOEP desorption from Au(111) is 145 kJ/mol. This value is significantly higher than for HOPG and qualitatively agrees with the DFT calculations[86] for CoOEP desorption into vacuum.

Given a better understanding of the formation and desorption kinetics of tectons, one may use their kinetics to create new self-assembled systems. An example of such kinetic control of a binary SAM is provided by CoOEP and coronene adsorbed from PO onto Au(111).[66] As we have shown above, CoOEP desorbs extremely slowly from gold below about 70 °C. Coronene, on the

DOI: 10.1021/acs.langmuir.7b02672
Langmuir 2018, 34, 3−17

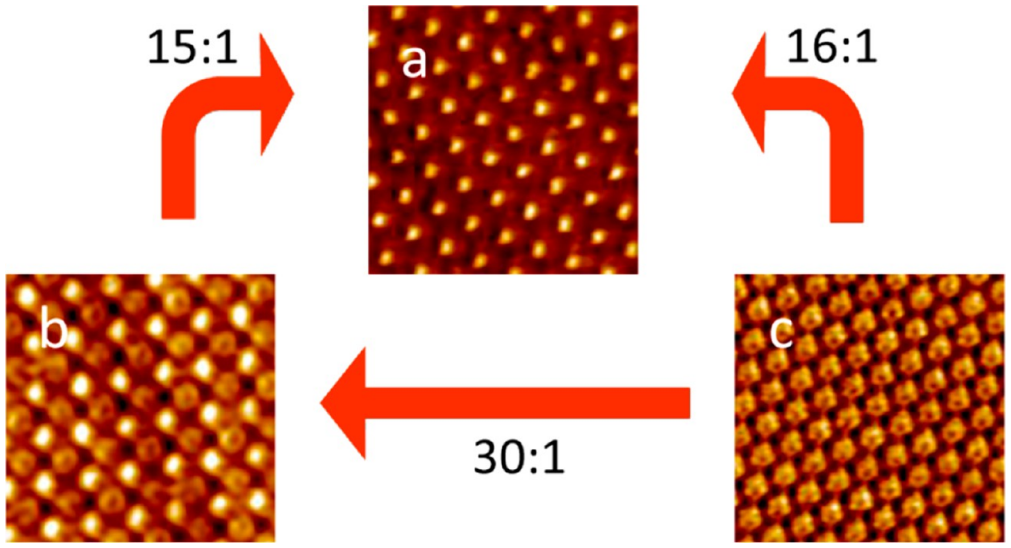


Figure 9. Changing the ratio of coronene to cobalt in the solution in contact with a given film structure on Au(111) could drive the surface in only one direction, toward the higher-concentration CoOEP phase. (a) CoOEP only, (b) 1−1 phase, and (c) pure coronene. The ratios shown are the coronene/CoOEP concentration ratios used to effect the conversions. Image reproduced from ref 66. Copyright 2015 American Chemical Society.

same surface, also desorbs slowly but is not as kinetically stable as is CoOEP.[49] Moreover, the solution-phase diffusion rates for CoOEP and coronene are similar.[66] Thus, the relative surface coverage and structure of any SAM formed will be strongly dependent on the concentrations of tectons in solution. As one varies the coronene to CoOEP ratio in PO from 0 to >60, the SAM structure evolves among only three unique structures with no sign of solid solution formation. These structures are shown in Figure 9. As long as the coronene/CoOEP ratio is less than about 20, only the dense CoOEP monolayer structure is observed (Figure 9a). If a clean Au(111) surface is exposed to a solution having a concentration ratio of between 23 and 40, only a new 1:1 rectangular structure spontaneously forms (Figures 3 and 9b). If the coronene/CoOEP ratio is in excess of about 56, only the coronene monolayer is present on the surface. In the narrow regions between these concentration ratio limits, phase segregation is seen. The coverage versus concentration plots derived by exposing clean Au(111) to various solution concentration ratios can be fit by a thermodynamic model. However, this would lead to invalid parameters because this system is not in thermodynamic equilibrium.

The simplest way to prove this system is not in equilibrium is to vary the solution concentration over the surface *after* a particular monolayer is formed. The change in surface structure with solution concentration ratio is ratchetlike. One finds that increasing the coronene concentration has no effect on any of the three structures, but increasing the CoOEP concentration in the covering solution does (Figure 9). A less-dramatic test is to monitor the 1:1 structure (Figure 9b) as a function of time and temperature. At 22 °C, it is stable for days. However, upon heating to 50 °C the 1:1 structure converts to pure CoOEP over the course of about 5.5 h. DFT studies on coronene and CoOEP on Au(111) indicate that the desorption energy in vacuum for coronene is considerably less than for CoOEP (2.4 eV versus 4.4 eV).[66] Jahanbekam et al. also showed that both of these values would be smaller but in similar proportion in solution.[66] Thus, given similar preexponential factors, the rate of desorption of coronene from Au(111) should be much larger than for CoOEP (as observed qualitatively[49]). In addition, the adsorption energy for coronene in the 1:1 structure is slightly greater than in the pure coronene phase.[66]

Jahanbekam and co-workers interpreted their observations and calculations to mean that the less-stable phases were formed at the nucleation stage and grew rapidly. Once the monolayer formed, coronene could very slowly desorb and be replaced by CoOEP, but the CoOEP did not desorb on the time scale of days. Thus, if the CoOEP impingement rate on the surface could be made higher than that of the coronene, then vacancies in the adlayer could be permanently filled by CoOEP. Adding to the stability of the coronene-containing phases is the size mismatch. A single desorbed coronene cannot be replaced by a CoOEP, which is too large to fit in the coronene footprint.

This system is unusual in several ways, but the absence of any significant lateral forces other than van der Waals and steric constraints is notable. Also notable is the fact that the construction of the well-ordered 1−1 adlayer requires that the components have solution concentrations differing by at least 1 order of magnitude. A critical element in this type of structure control is the fact that one component is irreversibly adsorbed. The authors suggest that new self-assembled structures may be formed through the use of conditions far from those frequently utilized.

3. KINETIC VERSUS THERMODYNAMIC CONTROL IN PORPHYRIN AND PHTHALOCYANINE MONOLAYER REACTIVITY

The reactivity of a SAM is of great importance in a number of applications. The ability to create sensitive chemical sensors and catalysts from SAMs depends strongly upon their surface reactivity. Optoelectronic and mechanical devices with exciting and unusual properties could result from the ability to extend a 2-D SAM design into three dimensions through vertical reaction chemistry. In the case of Pc and P SAMs, the most chemically accessible position is the central metal ion. MPc and MP systems are known to undergo axial coordination with multiple coordinating agents. Such coordination can provide the connection mechanism for the vertical replication of the SAM, or it can be the mechanism by which a species is sensed or activated for further chemical reaction. Thus, the coordination

DOI: 10.1021/acs.langmuir.7b02672
Langmuir 2018, 34, 3−17

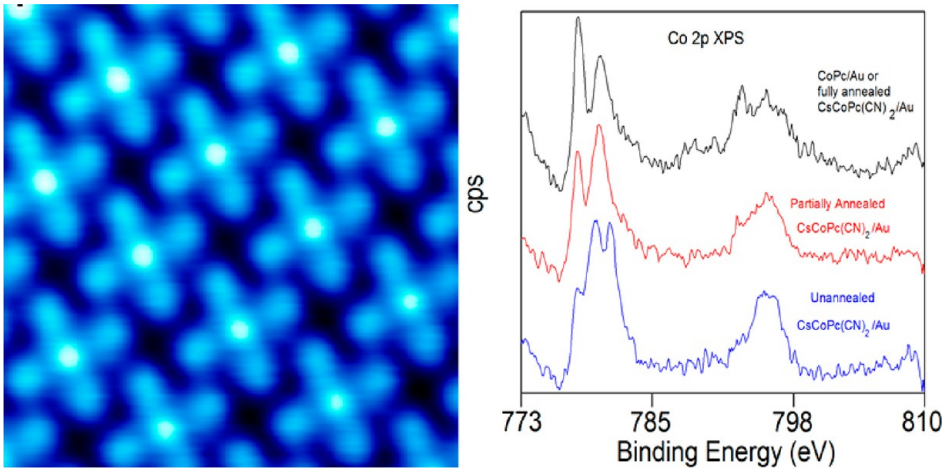


Figure 10. STM and XPS data obtained from $CsCoPc(CN)_2$ deposited on Au(111) from ethanol. The image was obtained under UHV conditions after annealing to 110 °C. XPS data show the transition from a mixture of cobalt(II) and cobalt(III) prior to annealing to all Co(II) following annealing to 110 °C. Data taken from ref 92. Copyright 2004 American Chemical Society.

chemistry of MP and MPc systems adsorbed on metal is of significant importance for many current and future technologies.

The coordination chemistry of metalloporphyrins (MP) and metallophthalocyanines (MPc) in solution is well known.[2] However, this wealth of chemical knowledge cannot be directly applied to MP and MPc systems adsorbed on a metal or HOPG surface because the interaction between the tecton and the substrate changes the reactivity of the metal ion. Initially, surface-dependent MPc and MP coordination chemistry was demonstrated in the UHV environment,[90,91] More recently, significant differences have been observed in reactions occurring in solution and at the solution−solid interface.[64,85,92,93]

An early example of MPc-substrate-driven chemistry was in the spontaneous reduction of biaxially substituted dicyano cobalt phthalocyanine salts, $MCoPc(CN)_2$ (M = K, Cs), by a gold substrate with the formation of a CoPc SAM.[92] The $MCoPc(CN)_2$ salt is chemically and thermally stable and soluble in a wide range of solvents, and its X-ray structure is known.[94] If a Au(111) surface is exposed to a solution of the salt in ethanol and then washed with ethanol, then an ordered monolayer is observed on the still-damp surface. STM measurements in air were unable to distinguish the adlayer from that of CoPc normally formed by vapor deposition in UHV. To better understand the SAM, it was transferred to UHV, where it was again imaged and X-ray photoelectron spectra (XPS) were recorded. The spectra indicated that the surface species was primarily a cobalt(II) complex with a contribution from cobalt(III) (Figure 10). The sample was then slowly heated to 110 °C with spectra acquired at various temperatures during the heating. By the time the sample reached 110 °C, the XPS was indistinguishable from that of an authentic CoPc sample. Furthermore, the N/C ratio determined by XPS of the fully annealed sample was the same as for authentic CoPc. Mazur and co-workers also measured the XPS in the Cs 3d region.[92] Because the sensitivity factor for Cs 3d is twice that for Co 3d, it would be very easy to detect as few as 1 cesium atom to 20 cobalt atoms in the film. No Cs signal was ever detected. Thus, the original adsorbed species was neutral, and the authors believed it was composed of a mixture of CoPc and CoPc(CN). With annealing, the residual CoPc(CN) decomposed to CoPc.

In this case, a species that was stable in solution decomposed to form a SAM. It is worth noting that once the SAM is formed, there is no further reduction. That is, no evidence for a second layer of any ethanol-insoluble species on the surface was observed. This is an additional confirmation that the chemistry is associated with the MPc/Au(111) interface. Once all the sites on the Au surface are occupied, the chemistry stops.

Perhaps the most detailed study to date of surface-specific chemistry concerns oxygen binding by CoOEP.[64] In fluid solution or in glasses, CoOEP will not bind oxygen at temperatures above 173 K. However, it is known that oxygen binding to cobalt porphyrins can be enhanced by axial coordination to a basic axial ligand (such as imidazole) at the position opposite to O_2 binding. Furthermore, cobalt porphyrins can act as oxidation catalysts in electrochemical cells. Thus, it seemed likely that a CoOEP SAM might display enhanced oxygen binding depending upon the substrate chosen. In the STM study by Mazur et al.,[64] oxygen partial pressure, temperature, and time were all treated as experimental parameters.

When CoOEP on HOPG is imaged in deoxygenated PO, all molecules appear bright. When O_2 is introduced, some go dim. These dim molecules were identified as those binding O_2 (as O_2^-). If one captures STM images of a given area with time, a movie results with molecules that appear to blink on and off. Each frame was analyzed for the fraction, θ, of dark molecules, and the values were plotted versus time.[64] This process is exemplified in Figure 11. Two of the images used to generate the indicated points are shown. In the first image, all the dim molecules have been indicated with a white circle. In the second image, those molecules that were dim in the previous image and remain dim are shown in white. The blue circles indicate dim molecules that were bright in the previous image. The scatter in the θ data is consistent with the expected statistical fluctuation of a small sample, $N^{-0.5}$. From this data, it is clear that the system is in dynamic equilibrium. Furthermore, if one changes the oxygen partial pressure over the solution, then the equilibrium shifts in concert. Thus, the system is in thermodynamic equilibrium.

Such time averages were collected for several partial pressures and several temperatures. It was found that the Langmuir isotherm well described the data. That is,

$$K = \frac{\theta}{(1-\theta)\left(\frac{P}{P^0}\right)} \tag{5}$$

DOI: 10.1021/acs.langmuir.7b02672
Langmuir 2018, 34, 3−17

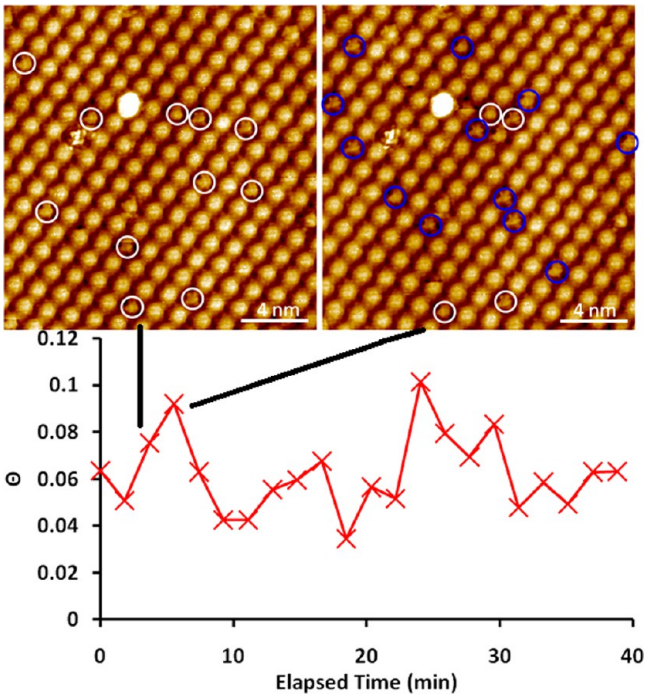


Figure 11. Time evolution of oxygen coverage on the CoOEP/HOPG surface in PO. θ is the fraction of CoOEP sites occupied by O_2 in a given frame. Two STM images are shown that were used to generate the indicated data points. Circled molecules indicate oxygen binding sites.

where P^0 is taken to be 1 Torr (which is conventional in the O_2 binding literature). From the Langmuir fits, Mazur obtained the equilibrium constant as a function of temperature for the process

$$O_{2(gas)} + CoOEP_{HOPG} = O_2CoOEP_{HOPG} \quad (6)$$

From $K(T)$, $\Delta G°(T) = -RT\ln(K(T))$ and $\Delta S° = -\left(\frac{\partial \Delta G°}{\partial T}\right)_p$ were used to determine $\Delta G° = 19$ kJ/mol, $\Delta S° = -297$ J/mol·K, and $\Delta H° = -68$ kJ/mol at 300 K. These values are in good agreement with those measured for systems that do bind O_2 in solution at room temperature. Note that the large positive value of $\Delta G°$ is a consequence of choosing a standard state where $\theta = 0.5$ when $P = 1$ Torr. A figure of merit often used in the O_2 binding field is $P_{1/2}$(25 °C). This is the partial pressure of O_2, expressed in Torr, that results in half of the metal porphyrins binding oxygen at any time. For CoOEP on HOPG, this value is 3200. Compared to cobalt myoglobin ($P_{1/2} = 57$), it seems very large, but there are designer cobalt porphyrins with $P_{1/2}$ values greater than 10 000.[95]

These results were qualitatively explained as follows: The HOPG acts as an electron donor to the porphyrin that in turn donates charge to form bound O_2^-. That is, HOPG is playing the role of an axial basic ligand in the overall complex. This picture suggests that the CoOEP support should play a significant role in oxygen binding. As an indicator of support donor activity, Hipps and co-workers selected the surface work function as a rough approximation. Supports with large work functions should be poor donors, and CoOEP supported on these surfaces should not bind oxygen. Those with small work functions should be effective electron donors, and CoOEP supported on these surfaces should bind oxygen well. Figure 12 shows the results of testing this hypothesis

CoOEP in PO was allowed to form monolayers on Au(111), HOPG, and MoS_2 under ambient conditions. These supports

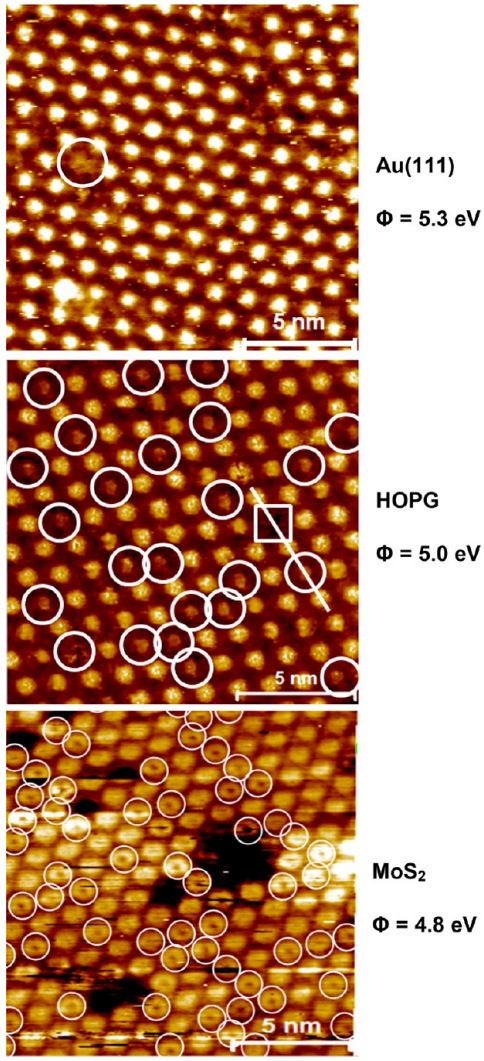


Figure 12. Drift-corrected constant-current STM images of supported CoOEP in PO under ambient conditions. Circles identify the oxygenated CoOEP molecules.

have progressively diminishing work functions, with Au(111) having the largest. Representative STM images are presented in Figure 12. Generally, all of the molecules looked bright on Au(111) with an occasional dim spot that could be an impurity in the original compound. On HOPG, we observed about 18% of the molecules bound to oxygen. In the case of MoS_2, the number of bound molecules increased to 34%. Thus, there is a very clear dependence on substrate.

It is interesting to note that whereas the oxygen-bound CoOEP on HOPG appears as dim spots, they appear to be donut-shaped on MoS_2. The latter result is reminiscent of the dark vanadyl phthalocyanine centers appearing in STM images due to oxygen's lack of states near the Fermi level.[46]

Another example of support-induced chemistry is the reaction of imidazole with NiOEP/HOPG in PO.[85] In solution at room temperature, imidazole does not coordinate with NiOEP even when the imidazole is present in a 50:1 molar excess. On the other hand, STM studies reveal that imidazole in PO solutions at the 1.5 mM level produces a $\theta = 0.5$ coverage at 25 °C. Like the O_2/CoOEP/HOPG system, creating an STM movie of surface complexation reveals that there is a time-varying distribution of bright and dim spots with a well-defined average associated with

DOI: 10.1021/acs.langmuir.7b02672
Langmuir 2018, 34, 3−17

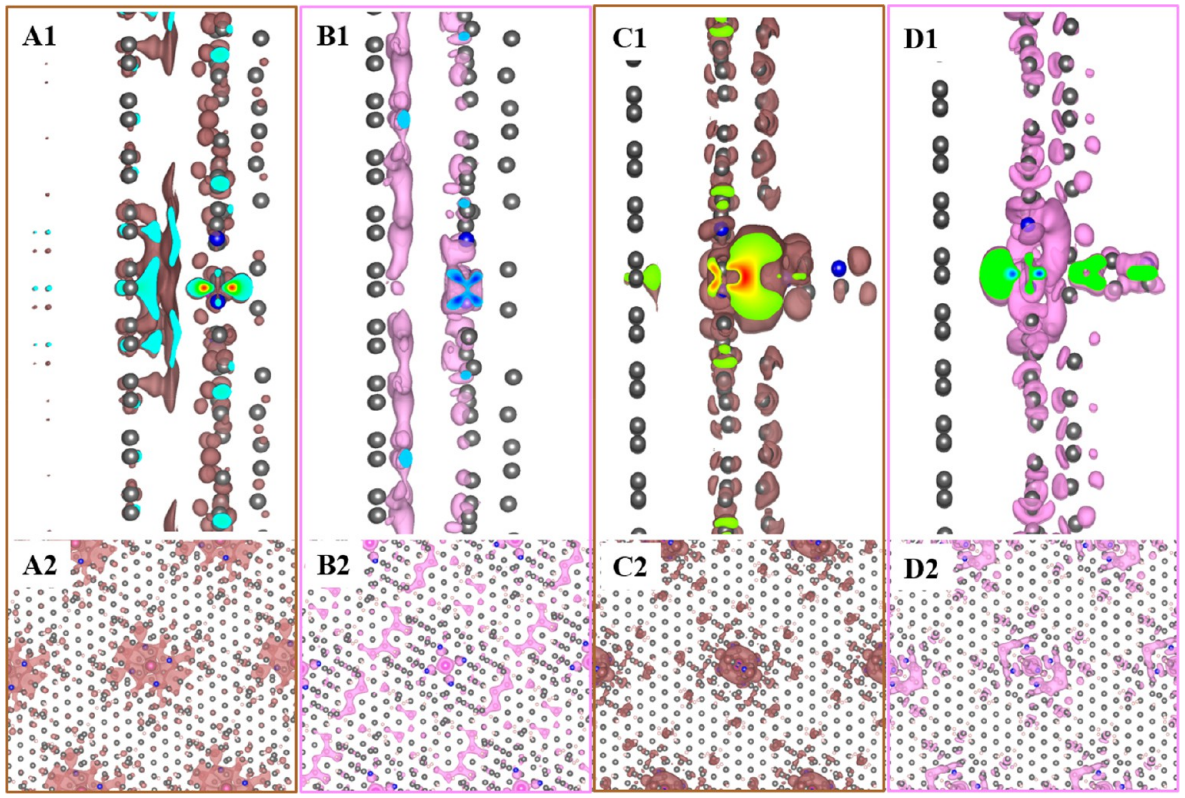


Figure 13. Charge density difference mappings for positive (colored in brown) and negative (colored in pink) charges for NiOEP/HOPG (A and B) and Im−NiOEP/HOPG (C and D) systems, respectively. The images in the top row (A1−D1) represent the side view (along the *a* axis), and the images in the bottom row (A2−D2) represent the top view (along the *c* axis). Element colors are carbon, gray; nitrogen, blue; and nickel, yellow (not visible). Hydrogens are masked for clarity. In the cross-section (A1−D1, top row), the rainbow colors (blue to red) indicate charge, with blue being highly negative and red being highly positive. Reproduced from ref 85. Copyright 2016 The Royal Society of Chemistry.

each imidazole solution concentration. In this case, the dim molecules are the pristine NiOEP and the bright molecules are those where an imidazole is bound.

The Langmuir isotherm fits the data well and gives an equilibrium constant, $K_c = \frac{\theta}{(1-\theta)\left(\frac{c}{c^0}\right)}$, where c^0 is 1 M. Nandi et al. defined the standard Gibbs free energy to be $\Delta G_c^0 = -RT \ln(K_c)$ and found $\Delta G_c^0 = -15.8$ kJ/mol. They estimated the standard reaction entropy, ΔS_c^0, to be −216 J/mol·K, which resulted in $\Delta H_c^0 = -80$ kJ/mol.

In solution, imidazole (Im) is viewed as an electron-donating ligand when binding to nickel(II) complexes. Often this results in a spin change for the nickel from a singlet to a triplet. How then does this picture fit within the model used of oxygen binding where HOPG was viewed as an electron donor? To better understand the bonding, we turned to density functional theory.[85] In the gas phase, we found that Im prefers to coordinate to the Ni^{2+} in NiOEP in a triplet spin state. The energy of this triplet, while negative, is so small that at room temperature entropic terms would dominate, yielding a nonbonding system. The characteristic dome structure of the porphyrin is predicted in the high-spin five-coordinate Im−NiOEP adduct. Additionally, the valence charge redistribution for the isolated Im−NiOEP high-spin complex indicates a charge transfer of ∼0.2 e from imidazole to NiOEP. This is not the situation for the HOPG supported system.

PW-DFT simulations on HOPG, NiOEP/HOPG, and the Im−NiOEP/HOPG slab structures indicate that all of these have a singlet lower in energy than the triplet.[85] Hence, we propose that imidazole binds to NiOEP on HOPG in a singlet ground state, which is not favorable when NiOEP is the gas phase or in solution. We believe that the HOPG substrate aids the binding of the Im ligand to NiOEP by acting as a donor of charge. This assumption can be further justified by examining the charge distribution at the Im−NiOEP/HOPG interface (Figure 13). For the NiOEP/HOPG interface, positive charge (Figure 13a) is mostly located on the NiOEP monolayer and in its vicinity, whereas negative charge (Figure 13B) is located on the HOPG substrate. But in the Im−NiOEP/HOPG interface, the positive charge (Figure 13C) is reduced on the Im−NiOEP monolayer in comparison to negative charge (Figure 13D). In the Im−NiOEP/HOPG case, there is almost no negative charge on HOPG (Figure 13D) and a small positive charge (Figure 13C). To obtain quantitative data on charge redistribution, charge distributions were integrated above and below the interface between the monolayer (NiOEP or Im−NiOEP) and the HOPG substrate. It was found that at the NiOEP/HOPG interface HOPG gains a charge of ∼0.1 e for each NiOEP molecule. In the Im−NiOEP/HOPG case, HOPG donates charge of ∼0.4 e to each Im−NiOEP complex. Thus, HOPG acts as an acceptor of charge from NiOEP without imidazole but as a donor when Im−NiOEP is the adsorbate. The 0.4 e charge donated by HOPG to Im−NiOEP is shared only a little with the NiOEP parent and mostly goes to imidazole (∼0.3 e). This is an unexpected finding because imidazole is assumed to be primarily a two-electron-donating ligand, but when Im binds to NiOEP on HOPG, it acts as a π-electron acceptor.

DOI: 10.1021/acs.langmuir.7b02672
Langmuir 2018, 34, 3−17

4. CONCLUSIONS AND OUTLOOK

Porphyrins and phthalocyanines are powerful components for the formation of catalysts, sensors, photoelectronics, FETs, OLEDs, and other essential components of modern technology. To make the most effective devices from these compounds, a method of rational design of their spatial distribution is required. Self-assembly in 2D is such a method for creating designed monolayer films. Axial coordination on the 2D SAM offers a mechanism for the rational design of 3D materials. Optimizing 2D assembly requires an understanding of the role of kinetics and thermodynamics in the assembly process. Assembly at the solution−solid interface allows the facile and inexpensive production of such SAMs and even the extension to processes such as inkjet printing. In this article, we have considered the role of kinetics and thermodynamics in the formation of 2D SAMs and in the axial chemistry of these systems.

The structures of SAMs formed from porphyrins and phthalocyanines near room temperature are usually controlled by kinetics. They are remarkably hardy, and it is difficult to dissolve them from a gold or HOPG surface with the organic solvents normally used for SAM production without heating. Both experiment and theory indicate that they adsorb more strongly on gold than on HOPG. We showed that desorption kinetics can be used to create new surface structures with multiple components. In the case where the components desorb slowly and occupy different areas on the surface, the adsorption and nucleation rates, rather than equilibrium constants, can determine the surface structure. Because adsorption rates are driven by solution concentration, surface structures vary with relative component concentration in a way that may mimic equilibria but is not. It was noted that the concentration ratios needed to tune structures may range over orders of magnitude in order to achieve simple 1:1 surface structures.

Although we were able to use STM to determine desorption rates, this was contingent on having systems with appropriately slow rates. Furthermore, only k_{d3} was determined. If progress is to be made in first measuring and then understanding the role of adsorption and desorption kinetics in SAM formation, then all of the parameters indicated in Figure 5 are required. Future studies are needed with much faster (video) scan rate STM instrumentation.[96] Even with a 10 Hz scan speed, it may be difficult to distinguish more than the dominant mechanism (terrace versus island edge versus intraisland) for some tectons. For these systems, the STM measurements will need to be paired with high-speed statistical measurements based on fluorescence, absorbance, or surface plasmon resonance.

Metalloporphyrin and metallophthalocyanine SAMs do not have the same axial chemistry on conducting surfaces that they have in solution. We have shown examples of systems that are stable in solution but not on a gold surface and systems that are not stable in solution but are stable on HOPG or MoS_2. Sometimes the surface complex is kinetically driven, and other times it can be proven that the system is in thermodynamic equilibrium. Computational studies are underway to better understand the role of the substrate in determining the electronic and chemical properties of MP and MPc systems, most of which, to date, are in the vacuum environment.[85,86,90] It is extremely important that any future experimental studies ascertain that the system is in thermodynamic equilibrium rather than just at steady state. Ideally, one will watch the surface coverage of bound systems as a function of time and ensure that exchange is actually occurring between the solution and surface and that the number of reaction sites is correctly related to solution concentration. When the time dependence is too fast for this, it should at least be determined that the same surface exists independently of the solution exposure history of the sample.

To analyze the kinetic and thermodynamic data in a useful (transferrable) way, the role of the solvent must be included. A critical need, therefore, is to obtain solvent-dependent terms, both for the equilibrium systems and for the activated complex. There currently exist reports of the use of molecular mechanics and also ab initio free-energy simulations to estimate the equilibrium solvent effects,[70,97] but these are few and generally most reliable when the solvent orders on the bare substrate. To our knowledge, there have been no efforts to model the transition states important in the SAM formation/dissolution process. The development of good methods (±5 kJ/mol) for calculating solvent-dependent enthalpy terms and for estimating entropic terms is an area richly deserving of attention. In the future, both ab initio simulations and molecular mechanics simulations may prove to be valuable tools for understanding kinetic vs thermodynamic control.

AUTHOR INFORMATION

Corresponding Author

*E-mail: hipps@wsu.edu.

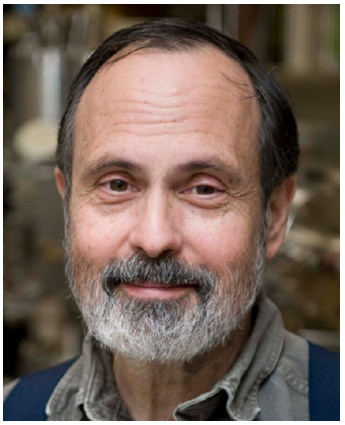
ORCID

K. W. Hipps: 0000-0002-5944-5114

Notes

The authors declare no competing financial interest.

Biographies



K. W. Hipps received his B.S. in chemistry from The University of Texas at El Paso. His Ph.D. is in chemical physics, and his dissertation was on magnetically induced circular polarization of emission. He won an NSF Postdoctoral Fellowship that he took to the University of Michigan, where he studied microwave−optical double-resonance spectroscopy. He is a Regents Professor of Chemistry and of Materials Science and Engineering at Washington State University in Pullman, Washington. Over the years, his interests have included microwave−optical double resonance, thermal modulation spectroscopy, determining excited-state geometries from the vibronic structuring of emission, Raman spectroscopy, inelastic electron tunneling spectroscopy for probing optically forbidden transitions, scanning tunneling microscopy, elastic tunneling spectroscopy, and XPS. His current interests include processes at the solution−conductor interface and nanocrystalline porphyrinic materials.

DOI: 10.1021/acs.langmuir.7b02672
Langmuir 2018, 34, 3−17



Ursula Mazur received her B.S. in chemistry from Wayne State University in Detroit and her Ph.D. in physical inorganic chemistry from the University of Michigan at Ann Arbor, where her dissertation was on the microwave spectroscopy of ozonides. She currently holds the rank of Full Professor of Chemistry and Materials Science and Engineering at Washington State University. Past interests included applications of inelastic electron tunneling spectroscopy to inorganic materials, purification and properties of cyanocarbons, and luminescence spectroscopy. Her current interests include chemical reactions at surfaces, structure–function relationships in porphyrinic nanocrystalline materials, and 2D metal–organic self-assembled structures. She is a Fellow of the ACS and of the AAAS.

■ ACKNOWLEDGMENTS

This material is based on work supported by the National Science Foundation under grant CHE-1403989. We gratefully acknowledge their support.

■ REFERENCES

(1) *Journal of Porphyrins and Phthalocyanines*; World Scientific, 1997 to present.
(2) *Handbook of Porphyrin Science*, Ed: Kadish, K., Guilard, R., Smith, K. World Scientific: Singapore, 2010; Vols. *1–44*.
(3) Gregory, P. Industrial applications of phthalocyanines. *J. Porphyrins Phthalocyanines* **2000**, *4*, 432–437.
(4) Gao, D.; Li, B.; Zheng, C.; Zhu, J.; Huang, W. Porphyrin Derivatives for Interfacial Modification of Hole Transport Layer/Perovskite Layer in Inverted Perovskite Solar Cells. *Faming Zhuanli Shenqing*, 2017, CN 106531888A.
(5) Imahori, H.; Umeyama, T.; Ito, S. Large π-Aromatic Molecules as Potential Sensitizers for Highly Efficient Dye-Sensitized Solar Cells. *Acc. Chem. Res.* **2009**, *42*, 1809–1818.
(6) Urbani, M.; Gratzel, M.; Nazeeruddin, M.; Torres, T. Meso-Substituted Porphyrins for Dye-Sensitized Solar Cells. *Chem. Rev.* **2014**, *114*, 12330–12396.
(7) Lvova, L.; Mastroianni, M.; Di Natale, C.; Lundstroem, I.; Paolesse, R. Towards hyphenated sensors development: Design and application of porphyrin electropolymer materials. *Electroanalysis* **2012**, *24*, 776–789.
(8) Zhai, J.; Li, H.; Sun, X. A novel application of porphyrin nanoparticles as an effective fluorescent assay platform for nucleic acid detection. *RSC Adv.* **2011**, *1*, 36–39.
(9) Lvova, L.; Pudi, R.; Galloni, P.; Lippolis, V.; Di Natale, C.; Lundstrom, I.; Paolesse, R. Multi-transduction sensing films for electronic tongue applications. *Sens. Actuators, B* **2015**, *207*, 1076–1086.
(10) Kralova, J.; Kejik, Z.; Briza, T.; Kaplanek, R.; Zaruba, K.; Martasek, P.; Kral, V.Design, Synthesis, Selective Recognition Properties and Targeted Drug Delivery Application. *Handbook of Porphyrin Science*; World Scientific, 2014; Vol. 33, pp 1–7510.1142/9789814417297_0008.
(11) Lukyanets, E. A. Phthalocyanines as photosensitizers in the photodynamic therapy of cancer. *J. Porphyrins Phthalocyanines* **1999**, *3*, 424–432.
(12) Kuznetsova, J. O.; Makarov, V. I. Application of nano-photosensitizers (aluminum phthalocyanine nanoparticles) for early diagnosis and prevention of inflammatory diseases. *J. Phys.: Conf. Ser.* **2016**, *737*, 012049.
(13) Hasobe, T. Self-Assembled Composite Materials of Porphyrins for Optoelectronics. *Multiporphyrin Arrays*; Kim, D., Ed.; 2012; pp 499–536.
(14) Jung, S.; Ha, C. Application of phthalocyanine derivatives as hole transporting layer to organic light emitting devices. *J. Nanosci. Nanotechnol.* **2008**, *8*, 4644–4648.
(15) Huang, X.; Zhu, C.; Zhang, S.; Li, W.; Guo, Y.; Zhan, X.; Liu, Y.; Bo, Z. Porphyrin-dithienothiophene π-conjugated copolymers: Synthesis and their applications in Field-Effect Transistors and Solar Cells. *Macromolecules* **2008**, *41*, 6895–6902.
(16) Gu, D.; Chen, Q.; Tang, X.; Gan, F.; Shen, S.; Liu, K.; Xu, H. Application of phthalocyanine thin films in optical recording. *Opt. Commun.* **1995**, *121*, 125–9.
(17) Zhang, X.; Yu, L.; Li, R.; Peng, T.; Li, X. Asymmetry and electronic directionality: a means of improving the red/near-IR-light-responsive photoactivity of phthalocyanine-sensitized carbon nitride. *Catal. Sci. Technol.* **2014**, *4*, 3251–3260.
(18) Guo, Y.; Xie, W.; Chen, L.; Peng, B. Preparation, characterization and application of multi-walled CNTs by phthalocyanine pyrolysis. *Huaxue Wuli Xuebao* **2004**, *17*, 767–774.
(19) Seo, S.; Lee, K.; Min, M.; Cho, Y.; Kim, M.; Lee, H. A molecular approach to an electrocatalytic hydrogen evolution reaction on single-layer graphene. *Nanoscale* **2017**, *9*, 3969–3979.
(20) Kraft, A. Organic field-effect transistors. The breakthrough at last. *ChemPhysChem* **2001**, *2*, 163–165.
(21) Zhang, Y.; Cai, X.; Bian, Y.; Jiang, J. Organic semiconductors of phthalocyanine compounds for field effect transistors (FETs). *Struct. Bonding (Berlin, Ger.)* **2010**, *135*, 275–322.
(22) Chae, S.; Kim, H.; Kim; Jun, Y.; Kim, S.; Kim, Y.; Lee, S. Preparation of new semiconducting tetraphenylethynyl porphyrin derivatives and their high-performing organic field-effect transistors. *Synth. Met.* **2016**, *220*, 20–24.
(23) Katz, H. E.; Huang, J. Thin Film Organic Electronics. *Annu. Rev. Mater. Res.* **2009**, *39*, 71–92.
(24) Oshiro, T.; Backstrom, A.; Cumberlidge, A.; Pevovar, S.; Bahr, D.; Smieja, J.; Hipps, K. W.; Mazur, U. Nanomechanical properties of highly ordered phthalocyanine Langmuir-Blodgett layers. *J. Mater. Res.* **2004**, *19*, 1461–1470.
(25) Duhm, S.; Heimel, G.; Salzmann, I.; Glowatzki, H.; Johnson, R. L.; Vollmer, A.; Rabe, J.; Koch, N. Orientation-dependent ionization energies and interface dipoles in ordered molecular assemblies. *Nat. Mater.* **2008**, *7*, 326–332.
(26) Wang, S.; Kiersnowski, A.; Pisula, W.; Mullen, K. Microstructure evolution and device performance in solution-processed polymeric field-effect transistors: The key role of the first monolayer. *J. Am. Chem. Soc.* **2012**, *134*, 4015–4018.
(27) Ding, S.-S.; Huang, W.-Q.; Yang, Y.; Zhou, B.; Hu, W.; Long, M.; Peng, P.; Huang, G. Dual role of monolayer MoS2 in enhanced photocatalytic performance of hybrid MoS2/SnO2 nanocomposite. *J. Appl. Phys.* **2016**, *119*, 205704.
(28) Ihm, K.; Kim, B.; Kang, T.; Kim, J.; Joo, M. H.; Kim, T.; Yoon, S.; Chung, S. Molecular orientation dependence of hole-injection barrier in pentacene thin film on the Au surface in organic thin film transistor. *Appl. Phys. Lett.* **2006**, *89*, 033504–033503.
(29) Lee, S. S.; Loth, M. A.; Anthony, J.; Loo, Y.-L. Orientation-independent charge transport in single spherulites from solution-processed organic semiconductors. *J. Am. Chem. Soc.* **2012**, *134*, 5436–5439.
(30) Liscio, F.; Albonetti, C.; Broch, K.; Shehu, A.; Quiroga, S.; Ferlauto, L.; Frank, C.; Kowarik, S.; Nervo, R.; Gerlach, A.; Milita, S.; Schreiber, F.; Biscarini, F. Molecular reorganization in organic field-

DOI: 10.1021/acs.langmuir.7b02672
Langmuir 2018, 34, 3–17

effect transistors and its effect on two-dimensional charge transport pathways. *ACS Nano* **2013**, *7*, 1257−1264.
(31) Wen, Y.; Chen, J.; Zhang, L.; Sun, X.; Zhao, Y.; Guo, Y.; Yu, G.; Liu, Y. Quantitative analysis of the role of the first layer in p- and n-Type organic field-effect transistors with graphene electrodes. *Adv. Mater.* **2012**, *24*, 1471−1475.
(32) Rabe, J. P. Self-assembly of single macromolecules at surfaces. *Curr. Opin. Colloid Interface Sci.* **1998**, *3*, 27−31.
(33) Hipps, K. W.; Scudiero, L.; Barlow, D.; Cooke, M. P. A self-organized 2-dimensional bi-functional structure formed by supra-molecular design. *J. Am. Chem. Soc.* **2002**, *124*, 2126−27.
(34) Whitesides, G. M.; Mathias, J.; Seto, C. Molecular self-assembly and nanochemistry: A chemical strategy for the synthesis of nanostructures. *Science* **1991**, *254*, 1312−1319.
(35) Florio, G.; Werblowsky, T.; Muller, T.; Berne, B.; Flynn, G. W. The self-assembly of small polycyclic aromatic hydrocarbons on graphite: A combined scanning tunneling microscopy and theoretical approach. *J. Phys. Chem. B* **2005**, *109*, 4520−4532.
(36) Amabilino, D. B. *Supramolecular Chemistry at Surfaces*; Royal Society of Chemistry: Cambridge, 2016.
(37) Scudiero, L.; Hipps, K. W.; Barlow, D. A self-organized 2-Dimensional bifunctional structure. *J. Phys. Chem. B* **2003**, *107*, 2903−2909.
(38) De Feyter, S.; De Schryver, F. Self-assembly at the liquid/solid interface: STM Reveals. *J. Phys. Chem. B* **2005**, *109*, 4290−4302.
(39) Iritani, K.; Tahara, K.; De Feyter, S.; Tobe, Y. Host−guest chemistry in integrated porous space formed by molecular self-assembly at liquid−solid Interfaces. *Langmuir* **2017**, *33*, 4601−4618.
(40) Wang, D.; Wan, L.; Bai, C.-L. Formation and structural transition of molecular self-assembly on solid surface investigated by scanning tunneling microscopy. *Mater. Sci. Eng., R* **2010**, *70*, 169−187.
(41) Barth, J.; Costantini, G.; Kern, K. Engineering atomic and molecular nanostructures at surfaces. *Nature* **2005**, *437*, 671−679.
(42) Santato, C.; Cicoira, F.; Rosei, F. Self-assembly of thiophene-based materials: a scanning tunneling microscopy perspective. *Handbook of Thiophene-Based Materials* **2009**, *2*, 517−547.
(43) Imahori, H.; Umeyama, T.; Kurotobi, K.; Takano, Y. Self-assembling porphyrins and phthalocyanines for photoinduced charge separation and charge transport. *Chem. Commun.* **2012**, *48*, 4032.
(44) Berner, S.; Lidbaum, H.; Ledung, G.; Ahlund, J.; Nilson, K.; Schiessling, J.; Gelius, U.; Backvall, J.; Puglia, C.; Oscarsson, S. Electronic and structural studies of immobilized thiol-derivatized cobalt porphyrins on gold surfaces. *Appl. Surf. Sci.* **2007**, *253*, 7540−7548.
(45) Long, R.; Casanova, D.; Fang, W.; Prezhdo, O. Donor−Acceptor Interaction Determines the Mechanism of Photoinduced Electron Injection from Graphene Quantum Dots intoTiO_2: π-Stacking Supersedes Covalent Bonding. *J. Am. Chem. Soc.* **2017**, *139*, 2619−2629.
(46) Mazur, U.; Hipps, K. W.; Riechers, S. Organization of Vanadyl and metal-free tetraphenoxyphthalocyanine complexes on highly oriented pyrolytic graphite in the presence of paraffinic solvents: A STM study. *J. Phys. Chem. C* **2008**, *112*, 20347−20356.
(47) Mamdouh, W.; Uji-i, H.; Ladislaw, J.; Dulcey, A.; Percec, V.; De Schryver, F.; De Feyter, S. Solvent controlled self-assembly at the liquid-solid interface revealed by STM. *J. Am. Chem. Soc.* **2006**, *128*, 317−325.
(48) Takami, T.; Mazur, U.; Hipps, K. W. Solvent-induced variations in surface structure of a 2,9,16,23-tetra-tert-butyl-phthalocyanine on graphite. *J. Phys. Chem. C* **2009**, *113*, 17479−17483.
(49) English, W. E.; Hipps, K. W. Stability of a surface adlayer at elevated temperature: Coronene and heptanoic acid on Au(111). *J. Phys. Chem. C* **2008**, *112*, 2026−2031.
(50) Venkataraman, B.; Breen, J.; Flynn, G. W. Scanning tunneling microscopy studies of solvent effects on the adsorption and mobility of Triacontane/Triacontanol molecules adsorbed on graphite. *J. Phys. Chem.* **1995**, *99*, 6608−6619.
(51) Gutzler, R.; Cardenas, L.; Rosei, F. Kinetics and thermodynamics in surface-confined molecular self-assembly. *Chemical Sciences* **2011**, *2*, 2290−2300.
(52) Pineider, F.; Mannini, M.; Sessoli, R.; Caneschi, A.; Barreca, D.; Armelao, L.; Cornia, A.; Tondello, E.; Gatteschi, D. Solvent effects on the adsorption and self-organization of Mn_{12} on Au(111). *Langmuir* **2007**, *23*, 11836−11843.
(53) Lippel, P. H.; Wilson, R.; Miller, M.; Woll, C.; Chiang, S. High-resolution imaging of copper-phthalocyanine by scanning-Tunneling Microscopy. *Phys. Rev. Lett.* **1989**, *62*, 171−174.
(54) Marbach, H.; Steinruck, H.-P. Studying the dynamic behaviour of porphyrins as prototype functional molecules by scanning tunneling microscopy close to room temperature. *Chem. Commun.* **2014**, *50*, 9034−9048.
(55) Lu, X.; Hipps, K. W.; Wang, X. D.; Mazur, U. Scanning tunneling microscopy of metal Phthalocyanines: d7 and d9 Cases. *J. Am. Chem. Soc.* **1996**, *118*, 7197−7202.
(56) Otsuki, J. STM studies of porphyrins. *Coord. Chem. Rev.* **2010**, *254*, 2311−2341.
(57) Qiu, X.; Wang, C.; Zeng, Q.; Xu, B.; Yin, S.; Wang, H.; Xu, S.; Bai, C. Alkane-assisted adsorption and assembly of Phthalocyanines and Porphyrins. *J. Am. Chem. Soc.* **2000**, *122*, 5550−5556.
(58) Shen, Y.; Deng, K.; Li, M.; Zhang, X.; Zhou, G.; Mullen, K.; Zeng, Q.; Wang, C. Self-assembling in fabrication of ordered porphyrins and phthalocyanines hybrid nano-arrays on HOPG. *CrystEngComm* **2013**, *15*, 5526−5531.
(59) Friesen, B.; Wiggins, B.; McHale, J.; Mazur, U.; Hipps, K. W. A Self-Assembled Two-Dimensional Zwitterionic Structure: H_6TSPP studied on HOPG. *J. Phys. Chem. C* **2011**, *115*, 3990−3999.
(60) Hipps, K. W.; Scudiero, L. Electron tunneling, a quantum probe for the quantum world of nanotechnology. *J. Chem. Educ.* **2005**, *82* (5), 704−711.
(61) den Boer, D.; Li, M.; Habets, T.; Iavicoli, P.; Rowan, A.; Nolte, R.; Speller, S.; Amabilino, D.; De Feyter, S.; Elemans, J. Detection of different oxidation states of individual manganese porphyrins during their reaction with oxygen at a solid/liquid interface. *Nat. Chem.* **2013**, *5*, 621−627.
(62) Claypool, C.; Faglioni, F.; Goddard, W., III; Gray, H. B.; Lewis, N.; Marcus, R. A. Source of image contrast in STM images of functionalized alkanes on graphite: A systematic functional group approach. *J. Phys. Chem. B* **1997**, *101*, 5978−5995.
(63) Hipps, K. W. Tunneling Spectroscopy of Organic Monolayers and Single Molecules. In *Topics of Current Chemistry: Unimolecular and Macromolecular Electronics II*; Metzger, R., Ed.; Springer Verlag, 2012.
(64) Friesen, B. A.; Bhattarai, A.; Hipps, K. W.; Mazur, U. Single molecule imaging of oxygenation of cobalt porphyrin at the solution/solid interface: Thermodynamics from microscopy. *J. Am. Chem. Soc.* **2012**, *134*, 14897−14904.
(65) Ogunrinde, A.; Hipps, K. W.; Scudiero, L. A Scanning tunneling microscopy study of self-assembled Nickel(II) octaethylporphyrin deposited from solutions on HOPG. *Langmuir* **2006**, *22*, 5697−5701.
(66) Jahanbekam, A.; Chilukuri, B.; Mazur, U.; Hipps, K. W. A Kinetically trapped two-component self assembled Adlayer. *J. Phys. Chem. C* **2015**, *119*, 25364−25376.
(67) Yoshimoto, S.; Honda, Y.; Osamu, I.; Itaya, K. Supramolecular Pattern of Fullerene on 2D Bimolecular "Chessboard" Consisting of Bottom-up Assembly of Porphyrin and Phthalocyanine Molecules. *J. Am. Chem. Soc.* **2008**, *130*, 1085−1092.
(68) Gentz, K.; Wandelt, K. Electrochemical STM: Atomic Structure of Metal/Electrolyte Interfaces. In *Fundamentals of Picoscience*; Sattler, K. D., Ed.; CRC Press, 2014; pp 269−286.
(69) Yuan, Q.; Xing, Y.; Borguet, E. An STM study of the pH dependent redox activity of a two dimensional hydrogen bonding porphyrin network at an electrochemical interface. *J. Am. Chem. Soc.* **2010**, *132*, 5054−5060.
(70) Song, W.; Martsinovich, N.; Heckl, W.; Lackinger, M. Born−Haber cycle for monolayer self-assembly at the liquid−solid interface: Assessing the enthalpic driving force. *J. Am. Chem. Soc.* **2013**, *135*, 14854−14862.
(71) Mazur, U.; Hipps, K. W. Kinetic and thermodynamic processes of organic species at the solution solid interface: The view through an STM. *Chem. Commun.* **2015**, *51*, 4737−4749.
(72) Hipps, K. W.; Bhattarai, A. Measuring Desorption Rates from Self-Assembled Monolayers at the Solution-Solid interface. In

DOI: 10.1021/acs.langmuir.7b02672
Langmuir 2018, 34, 3−17

Encyclopedia of Interfacial Chemistry: Surface Science and Electrochemistry; Wandelt, K.; 2017 (in press).
(73) Jung, L. S.; Campbell, C. T. Sticking probabilities in adsorption of alkanethiols from liquid ethanol solution onto gold. *J. Phys. Chem. B* **2000**, *104*, 11168−11178.
(74) Antczak, G.; Ehrlich, G. *Surface Diffusion: Metals, Metal Atoms, and Clusters*; Cambridge University Press: Cambridge, 2010.
(75) Eyring, H. The activated complex in chemical reactions. *J. Chem. Phys.* **1935**, *3*, 107−115.
(76) Coenen, M.; Cremers, M.; den Boer, D.; van den Bruele, F.; Khoury, T.; Sintic, M.; Crossley, M.; van Enckevort, W.; Hendriksen, W.; Elemans, J. A.; Spellera, S. Little exchange at the liquid/solid interface: defect-mediated equilibration of physisorbed porphyrin monolayers. *Chem. Commun.* **2011**, *47*, 9666−9668.
(77) Scudiero, L.; Barlow, D. E.; Hipps, K. W. Physical properties and metal ion specific scanning tunneling microscopy images of metal(II) tetraphenylporphyrins deposited from the vapor onto gold (111). *J. Phys. Chem. B* **2000**, *104*, 11899−11905.
(78) Bhattarai, A.; Mazur, U.; Hipps, K. W. A single molecule level study of the temperature dependent kinetics for the formation of metal porphyrin monolayers on Au(111) from solution. *J. Am. Chem. Soc.* **2014**, *136* (5), 2142−2148.
(79) Scudiero, L.; Barlow, D. E.; Hipps, K. W. Scanning tunneling microscopy, orbital mediated tunneling spectroscopy, and ultraviolet photoelectron spectroscopy of Nickel(II) octaethylporphyrin deposited from vapor. *J. Phys. Chem. B* **2002**, *106*, 996−1003.
(80) Karpovich, D. S.; Blanchard, G. J. Direct measurement of the adsorption kinetics of alkanethiolate self-assembled monolayers on a microcrystalline gold surface. *Langmuir* **1994**, *10*, 3315−3322.
(81) Jung, L.; Campbell, C. T. Sticking Probabilities in Adsorption of Alkanethiols from Liquid Ethanol Solution onto Gold. *J. Phys. Chem. B* **2000**, *104*, 11168−11178.
(82) Bhattarai, A.; Mazur, U.; Hipps, K. W. Desorption kinetics and activation energy for cobalt octaethylporphyrin from graphite at the phenyloctane solution-graphite interface: An STM study. *J. Phys. Chem. C* **2015**, *119*, 9386−9394.
(83) Bhattarai, A.; Marchbanks-Owens, K.; Mazur, U.; Hipps, K. W. Influence of the central metal ion in the desorption kinetics of a porphyrin from the solution/HOPG interface. *J. Phys. Chem. C* **2016**, *120*, 18140−18150.
(84) Campbell, C. T.; Arnadottir, L.; Sellers, J. Kinetic prefactors of reactions on solid surfaces. *Z. Phys. Chem.* **2013**, *227*, 1435−1454.
(85) Nandi, G.; Chilukuri, B.; Hipps, K. W.; Mazur, U. Surface directed reversible imidazole ligation to nickel(II) octaethylporphyrin at the solution/solid interface: a single molecule level study. *Phys. Chem. Chem. Phys.* **2016**, *18*, 20819−20829 Supplementary Materials..
(86) Chilukuri, B.; Mazur, U.; Hipps, K. W. Effect of dispersion on surface interactions of cobalt(II) octaethylporphyrin monolayer on Au(111) and HOPG(0001) substrates: A comparative first principles study. *Phys. Chem. Chem. Phys.* **2014**, *16*, 14096−14107.
(87) Jahanbekam, A. Temperature Dependent Stm Studies of Organic Molecules at the Solution/Solid Interface Including New Instrumental Development. Ph.D. Dissertation, 2015, Washington State University.
(88) Edwards, L.; Dolphin, D.; Gouterman, M. XVI. Vapor absorption spectra and redox reactions: Octaalkylporphyrins. *J. Mol. Spectrosc.* **1970**, *35*, 90−95.
(89) Chessick, J.; Zettlemoyer, A. C.; Yu, F. Free energies, heats, and entropies of wetting of graphite. *J. Phys. Chem.* **1960**, *64*, 530−531.
(90) Gottfried, M. J. Surface chemistry of porphyrins and phthalocyanines. *Surf. Sci. Rep.* **2015**, *70*, 259−379.
(91) Ballav, N.; Wackerlin, C.; Siewert, D.; Oppeneer, P.; Jung, T. Emergence of on-surface magnetochemistry. *J. Phys. Chem. Lett.* **2013**, *4*, 2303−2311.
(92) Mazur, U.; Leonetti, M.; English, W. A.; Hipps, K. W. Spontaneous solution phase redox deposition of a dense cobalt(II) phthalocyanine monolayer on gold. *J. Phys. Chem. B* **2004**, *108*, 17003−17006.
(93) Visser, J.; Katsonis, N.; Vicario, J.; Feringa, B. L. Two-Dimensional Molecular Patterning by Surface-Enhanced Zn-Porphyrin Coordination. *Langmuir* **2009**, *25*, 5980−5985.
(94) Inabe, T.; Maruyama, Y. Multi-dimensional stacking structures in phthalocyanine-based electrical conductors, K[Co(phthalocyanato)-$(CN)_2]_2 \cdot 5CH_3CN$ and Co(phthalocyanato)$(CN)_2 \cdot 2H_2O$. *Bull. Chem. Soc. Jpn.* **1990**, *63*, 2273−2280.
(95) Collman, J. P.; Brauman, J.; Doxee, K.; Halbert, T.; Hayes, S.; Suslick, K. Oxygen binding to cobalt porphyrins. *J. Am. Chem. Soc.* **1978**, *100*, 2761−2766.
(96) Yang, Y.; Magnussen, O. M. Quantitative studies of adsorbate dynamics at noble metal electrodes by in situ Video-STM. *Phys. Chem. Chem. Phys.* **2013**, *15*, 12480−12487.
(97) Reimers, J.; Panduwinata, D.; Visser, J.; Chin, Y.; Tang, C.; Goerigk, L.; Ford, M.; Sintic, M.; Sum, T.; Coenen, M.; Hendriksen, B.; Elemans, J.; Hush, N.; Crossley, M. A priori calculations of the free energy of formation from solution of polymorphic self-assembled monolayers. *Proc. Natl. Acad. Sci. U. S. A.* **2015**, *112*, E6101−E6110.

NOTE ADDED AFTER ASAP PUBLICATION

This paper was published ASAP on September 20, 2017 with errors in the text. The corrected version was reposted on October 26, 2017.

DOI: 10.1021/acs.langmuir.7b02672
Langmuir 2018, 34, 3−17